

PACS numbers: 42.55.Px; 42.60.Da; 42.60.Fc; 42.60.Lh
DOI: 10.1070/QE2014v044n11ABEH015618

Experimental study of a modulated beam AlGaAs/GaAs diode amplifier operating in the highly saturated gain regime

N.V. D'yachkov, A.P. Bogatov, T.I. Gushchik, A.E. Drakin

Abstract. **The variation in the modulation parameters of an optical signal in a diode power amplifier has been studied experimentally. The experimental data obtained agree well with theory that takes into account nonlinear interaction between fields in the gain medium of a laser through inversion beating. It is shown that the dominant type of output signal modulation is phase modulation, whose depth depends on the amplitude–phase coupling coefficient of the gain medium of the amplifier and the nature of the modulation (the phase relationships between the spectral components) of the output signal.**

Keywords: *diode optical amplifier, amplitude/phase modulation.*

1. Introduction

Calculation results [1] suggest that diode amplifiers have considerable potential for use as output amplifiers of modulated optical beam power in free-space optical communication systems. The calculations, based on theory developed previously [2], used a number of internal parameters of the gain medium of the diode laser. Even though those parameters were employed in many studies, a scatter in their values, due to the use of different gain media of diode lasers and specific design features, may add uncertainty to predicted results. In view of this, the conclusions drawn in Ref. [1] require experimental verification through comparison of the calculation results with experimental data.

There are currently no experimental data on the use of a diode amplifier in the highly saturated regime for amplifying optical beams modulated in the gigahertz range. It is only this regime that can ensure the highest electrical-to-optical power conversion efficiency.

In connection with this, the purpose of this work is to experimentally study the amplification of quasi-monochromatic optical radiation in a diode amplifier in the case of gain saturation by input light. Of particular interest is to obtain data on how beam modulation parameters vary when the beam passes through such an amplifier.

N.V. D'yachkov, A.P. Bogatov, T.I. Gushchik, A.E. Drakin
P.N. Lebedev Physics Institute, Russian Academy of Sciences, Leninsky prosp. 53, 119991 Moscow, Russia;
e-mail: kln4d@yandex.ru, bogatov@sci.lebedev.ru

Received 9 July 2014
Kvantovaya Elektronika **44** (11) 1005–1011 (2014)
Translated by O.M. Tsarev

2. Experimental setup

Figure 1 shows a simplified schematic of the experimental setup. Single-frequency external cavity diode laser (unit I) served as a master oscillator. Its output, whose spectrum is shown in the left inset, was fed to the input of a diode amplifier/modulator (unit II). The pump current of the amplifier/modulator had a controlled direct component and a controlled harmonic component at frequencies in the range $\Omega/2\pi = 400–1150$ MHz. As a result, the output emission spectrum of the amplifier/modulator contained the carrier frequency of the master oscillator, ω_0, and two side frequencies symmetric with respect to the carrier frequency, distance Ω from it (Fig. 1, right inset). This emission was directed through a plate beam splitter to the input of a diode power amplifier (unit III), which was the main subject of this study.

The principle and experimental realisation of a spectrally matched, modulated optical radiation source with the use of a single-frequency laser and diode amplifier/modulator (units I and II) were described previously (see e.g. Refs [2, 3]). Optical coupling between the units was ensured by a parallel beam focused by lenses (*4*, *5*) (collimators of the laser diode output).

All experiments were carried out for a spatial beam profile corresponding to a single transverse mode of the laser diodes (*1–3*). To ensure sharp beam focusing by lenses *4*, special attention was paid to the choice of the optics and positioning system of these lenses. In our case, an optimal solution was to use lens 'heads' from DVD players. All of them were controlled electromechanically using a computer. In the simplified schematic in Fig. 1, the control circuits of the positioning units and their interface with the computer are omitted. Lenses *5*, intended to produce a parallel beam at the output of the laser and amplifier diodes, were positioned manually before inserting the corresponding units in the optical system. The focal length of the lenses was ~3 mm, so that the linear dimensions of the optical beams in units I–III did not exceed 4 mm. Figure 2 shows the optical schemes of the master oscillator and amplifier module, indicates the precision lens positioning directions and specifies the accuracy in the position of the lenses. The diode heterostructure layers are parallel to the *yz* plane. Coarse positioning of the optical units was performed manually, via mechanical translation.

The cavity of the master oscillator (Fig. 2a) included, in addition to the mirrors formed by the diode facets, an external wavelength-selective mirror in the form of a total internal reflection holographic grating [4]. The zeroth order of the grating served as the optical output of the master oscillator. The light from the high-reflectivity mirror of the laser diode was used as an additional optical output to measure the laser

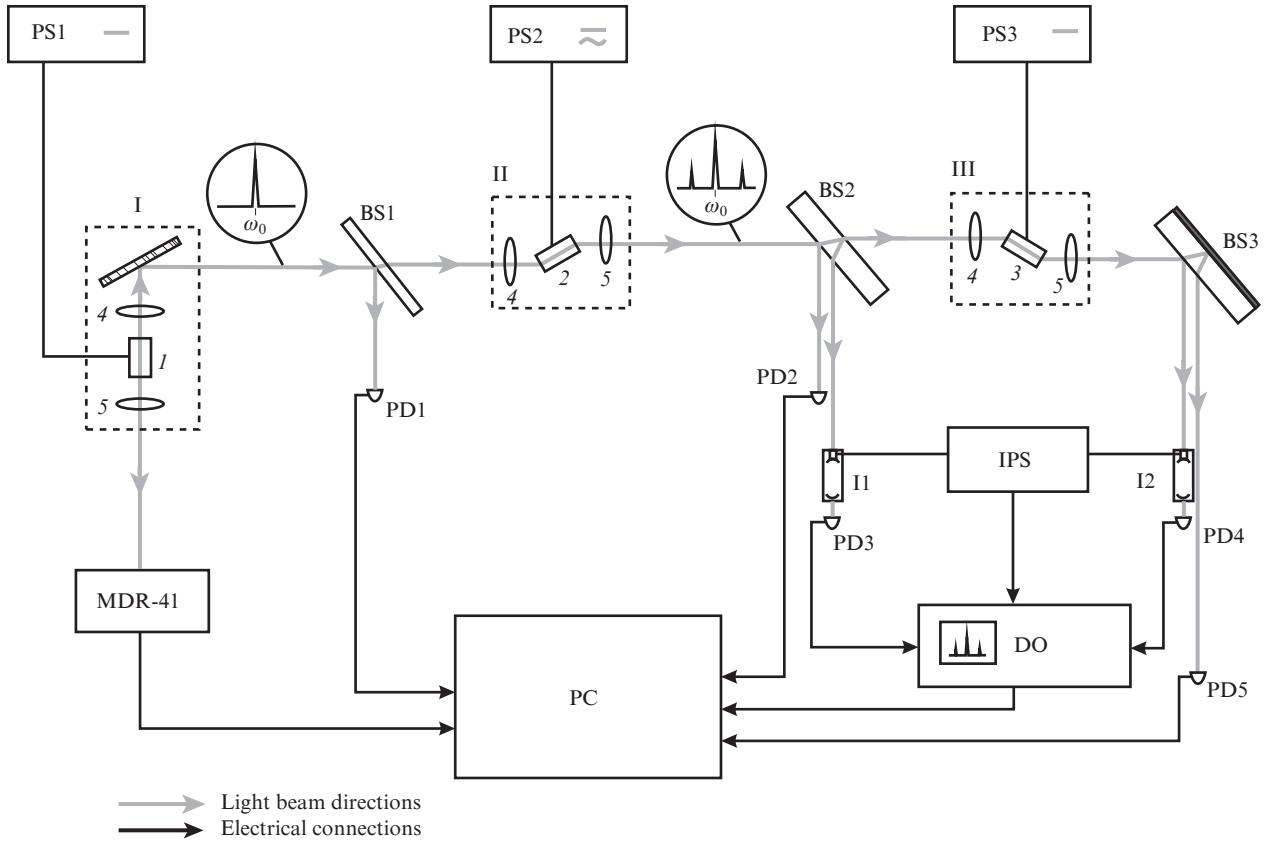

Figure 1. Schematic of the experimental setup: (I) single-frequency external-cavity laser unit; (II) diode amplifier/modulator unit; (III) diode power amplifier unit; (PS1–PS3) power supplies of the laser and amplifiers; (BS1–BS3) plate beam splitters; (I1, I2) confocal Fabry–Perot interferometers; (IPS) power supply of the interferometers; (MDR) MDR-41 monochromator; (PD1–PD5) photodiodes; (DO) V-423 digital oscilloscope; (PC) control computer; (1–3) laser diodes; (*4*, *5*) lenses.

spectrum with an MDR-41 monochromator, equipped with a computer-interfaced linear photodetector array (Fig. 1).

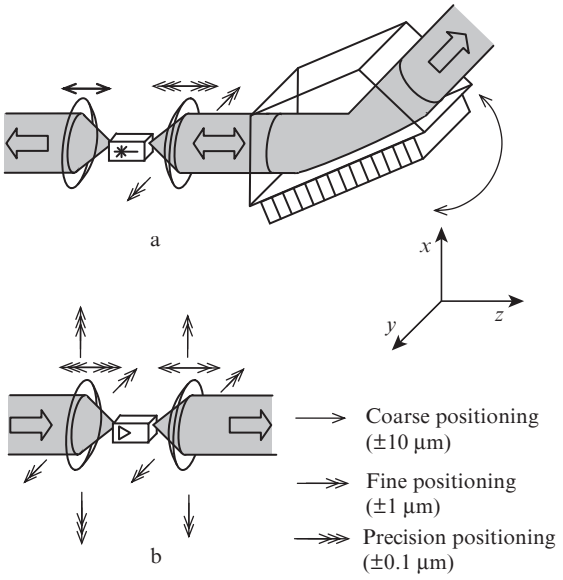

Figure 2. Optical schemes of the (a) single-frequency laser and (b) amplifier module. The thin arrows indicate the required lens positioning accuracy in the corresponding directions. The heterostructure layers (p–n junction) are parallel to the *yz* plane.

The laser diodes for the master oscillator and amplifiers were fabricated using AlGaAs/GaAs heterostructures intended for high-power single-transverse-mode lasers operating in the 850-nm spectral range. The geometry of the layers in the heterostructures was similar to that described elsewhere [5]. The main distinction of the amplifier diodes *2* and *3* from the laser diode *1* was that the optical axis of the active region of the amplifier diodes was inclined at ~7° to their facets, which had antireflection coatings. This made it possible to avoid self-oscillation of the amplifiers. The amplifier diodes were designed at Superlum Diodes Ltd. (Moscow). Their design was described previously [6], and some of their parameters are indicated in Table 1.

Table 1. Geometric and material parameters of the amplifier.

Parameter	Notation	Value
Optical confinement factor	Γ(%)	2.0
Thickness of the active region	d_a/nm	9.2
Ridge width	W/μm	5.0
Amplifier length	L/cm	0.16
Master oscillator wavelength	λ_0/nm	850

The input and output emission spectra of the power amplifier were obtained using scanning confocal interferometers (I1, I2). The interferometers were scanned by simultaneously applying a sawtooth voltage from the IPS to piezoceramic mirror mounts. The output of the interferometers was

detected by photodiodes (PD3, PD4), whose signals were fed to a V-423 digital oscilloscope, where the data were digitised before being fed to the computer, as schematised in Fig. 1. The input optical beams of the interferometers were produced by plate beam splitters (BS2, BS3).

Figure 3 shows typical spectra of the input and output beams, obtained using the scanning interferometers (I1, I2). The output signals of the interferometers are normalised to the intensity at the carrier frequency, which ensures that the amplitudes of the side peaks are the absolute squares ($|V_{\pm 1}|^2$) of the corresponding relative amplitudes of waves at the side frequencies $V_{\pm 1}(\Omega)$ determined in Ref. [1]. The linewidths in Fig. 3 correspond to the spectral resolution of the interferometers.

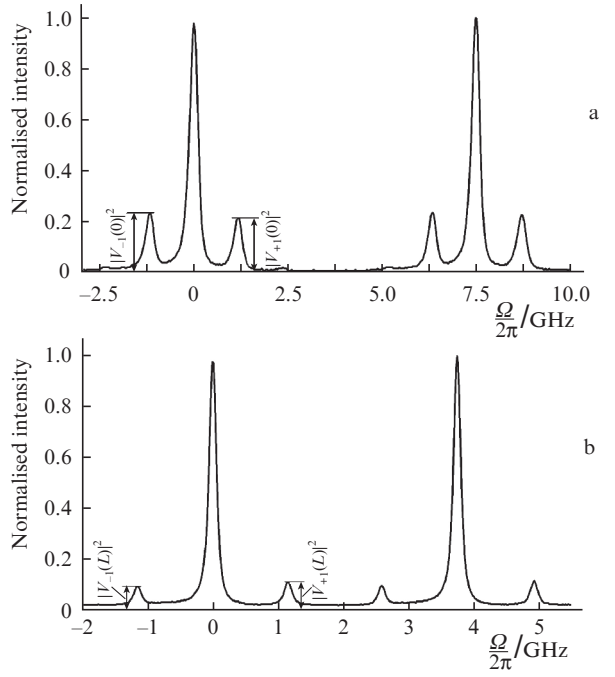

Figure 3. Typical spectra of the (a) input and (b) output optical beams. The spectra were obtained using the interferometers I1 (free spectral range of 7.5 GHz) and I2 (free spectral range of 3.75 GHz). Two transmission orders of the interferometers are shown.

The plate beam splitters (BS1–BS3) also produced beams for measuring the output power of the master oscillator and the input and output integrated powers of the amplifier under study with the use of photodiodes (PD1, PD2, PD5), whose signals were fed to the computer.

By varying the direct component of the pump current from the power supplies PS1 and PS2, the power of the input optical beam for the amplifier under study (unit III) was tuned over a necessary range. Varying the amplitude and frequency of the alternating component from PS2, we were able to tune the depth and frequency of its harmonic modulation.

Thus, the described experimental setup allowed the parameters of the input modulated optical beam of the amplifier and its operation conditions to be tuned over wide ranges by varying the pump current from PS3 and enabled all necessary measurements: those of the emission spectrum and the intensity of the beam every time it passed through the optical system.

3. Experimental results and analysis

In the first part of this study, our purpose was to measure static characteristics of the amplifier. In those measurements, the input beam was monochromatic light of constant intensity at the carrier frequency ω_0 of the master oscillator. The alternating component of the amplifier/modulator current (diode *2*) was then zero, and varying the direct component of the current, we were able to control the intensity of the input beam of the amplifier (diode *3*). Figures 4 and 5 present results of such studies.

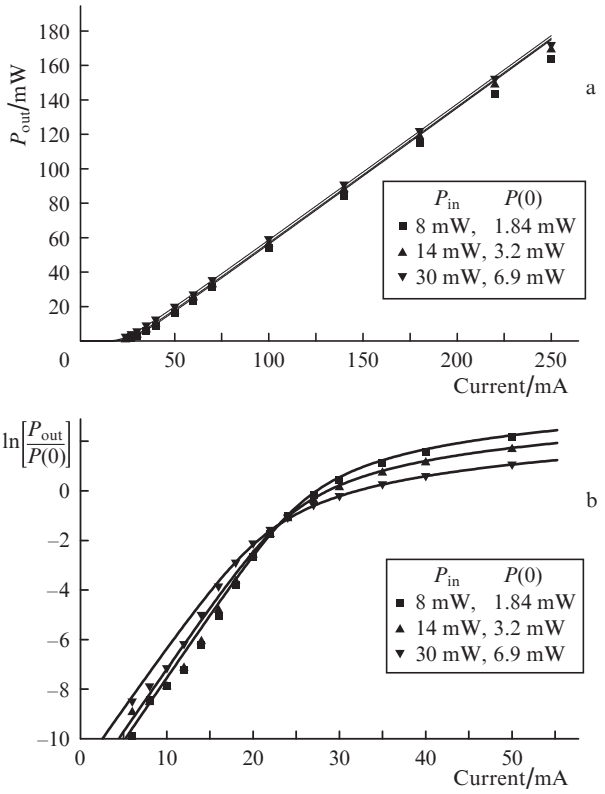

Figure 4. Power–current curves of the power amplifier (P_{out}) at different input powers (P_{in}). The experimental data (points) and calculation results (solid lines) are presented (a) on linear scales over the entire range of pump currents studied and (b) as a semilog plot at low pump currents.

Figure 4a shows typical power–current curves: output beam power P_{out} as a function of pump current J at different input beam powers $P(0)$. It is seen that the power–current characteristic is linear even at rather high currents J. First, this points to good calculation accuracy and adequacy of the approximation used in [1] for the output power of the amplifier as a function of pump current [Eqn (10)]. Second, taking the pump efficiency to be $\Gamma_w \cong 1$, which is quite reasonable for the type of laser diode under consideration, we can find the background loss α from the slope of the linear portion. From the data in Fig. 4a, we obtain $\alpha = 8.5\ \text{cm}^{-1}$.

Figure 4b presents results (in greater detail than in Fig. 4a) for the initial portion of the power–current characteristic (semilog plot). Using previous results [1], it can be shown that, at low currents, the slope of the linear portion of the curves in Fig. 4b is

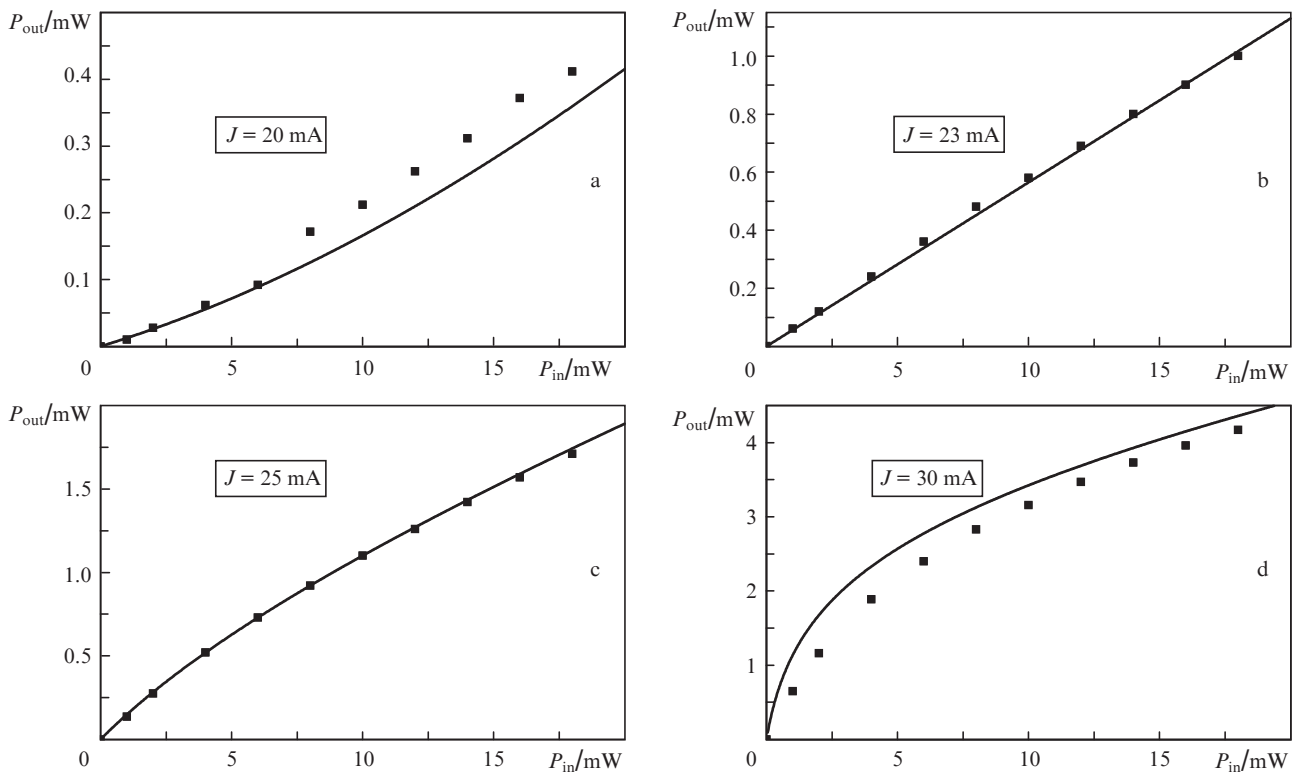

Figure 5. Output amplifier power P_{out} as a function of input beam power P_{in} at various pump currents.

$$\frac{d(\ln P_{out})}{dJ} = \left(\frac{\Gamma_w \Gamma}{e d_a W}\right)\sigma\tau . \quad (1)$$

From the data in Table 1 and Fig. 4b, we can directly find $\sigma\tau$. This product determines the saturation intensity, $I_s = h\omega_0 \times (\sigma\tau)^{-1}$, and hence the nonlinear portion of the curves in Fig. 4b. All this offers the possibility to evaluate, using the data in Fig. 4b, not only the $\sigma\tau$ product but also the optical power coupling efficiency from the parallel beam to the optical waveguide of the amplifier (κ) and the transparency current (J_{tr}) by fitting experimental data with calculation results. This can be done because all these coefficients correspond to various properties of the function $P_{out}(J)$ and are thus linear-independent. In Fig. 4, κ is already used to convert the measured power incident on the amplifier to the input beam power $P(0)$ in the amplifier. The accuracy in the values of $\sigma\tau$, κ and J_{tr} thus determined proved to be quite acceptable for further analysis because, in our measurements, P_{out} was varied over more than four orders of magnitude.

This is supported by the data in Fig. 5, which can be used to independently determine the transparency current J_{tr} and coupling efficiency κ. Indeed, P_{out} should be a linear function of $P(0)$ near the transparency current ($J \approx J_{tr}$), a sublinear function for $J > J_{tr}$ and superlinear for $J < J_{tr}$. Such behaviour can be seen in Fig. 5 at J_{tr} = 23 mA. From the data in Fig. 4b, we obtain $J_{tr} = 23.2 \pm 1$ mA (the range that includes all the intersections of the three experimental curves). From the slope of the straight line in Fig. 5b, evaluated for the input beam power outside the amplifier, we obtain $\kappa = 0.22$, in good agreement with the $\kappa = 0.23$ extracted from the data in Fig. 4b. Table 2 lists experimentally determined static parameters of the amplifiers studied. The estimated error does not considerably exceed the scatter in the other parameters of the amplifiers, e.g. geometric and optical, presented in Table 1 for similar laser diodes.

Table 2. Parameters derived by analysing static characteristics of the amplifier.

Parameter	Notation	Value
'Dynamic' stimulated transition cross section	$\sigma\tau$/ns cm^2	1.9×10^{-15}
Transparency current	J_{tr}/mA	23.0
Background loss coefficient in the waveguide	α/cm^{-1}	8.5
Coupling efficiency for the amplifier	κ (%)	23
Gain saturation intensity	I_s/kW cm^{-2}	123
Gain saturation power	P_s/mW	2.83

Thus, the above results strongly suggest, first, that the theory presented in Refs [1, 2] and related calculations adequately describe the behaviour of the static characteristics of the amplifier and, second, that these results make it possible to find those parameters of the amplifier determining its dynamic characteristics.

Our results on dynamic characteristics are presented below. The main measurands in our experiments were the beam powers at the amplifier input and output, $P(0)$ and P_{out}, and the ratios of the powers at the side frequencies, $P(\omega_0 \pm \Omega)$, to the power of a wave at the carrier frequency, $P(\omega_0)$:

$$|V_{\pm 1}|^2 = \frac{P(\omega_0 \pm \Omega)}{P(\omega_0)} \quad (2)$$

In our experiments, the absolute squares $|V_{\pm 1}|^2$ were found as the amplitudes of the side peaks in the interferometer signal, normalised to the amplitude of the peak corresponding to the carrier (centre) frequency (Fig. 3). In comparing experimental

data and calculation results, $|V_{\pm1}|^2$ was calculated using Eqn (15) from Ref. [1].

Figure 6 illustrates the effect of P_{out} (which was varied by changing the pump current of the amplifier) on the ratio of the powers at the side frequencies at the amplifier output ($z = L$) to that at the amplifier input ($z = 0$): $|V_{\pm1}(L)|^2/|V_{\pm1}(0)|^2$. The parameter of these dependences is the modulation frequency. It is seen that calculation results are in reasonable agreement with experimental data.

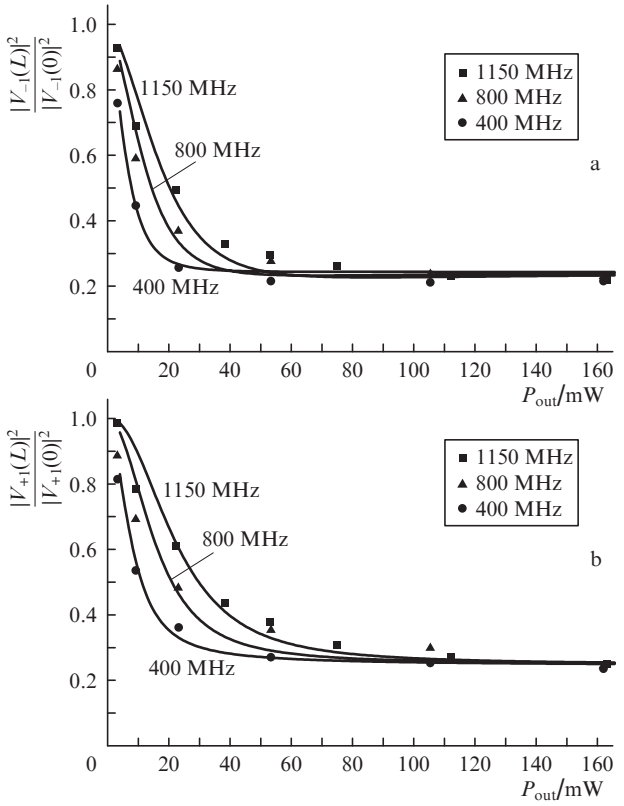

Figure 6. Relative change in the absolute squares of the amplitudes of the (a) Stokes and (b) anti-Stokes components for amplification in the power amplifier at an input power of 3.2 mW and different input beam modulation frequencies. The direct component of the pump current through the amplifier/modulator is 110 mA. The points represent the experimental data and the solid lines show calculation results at $\tau = 1.6$ ns and amplitude–phase coupling coefficients of the amplifier/modulator and power amplifier $R_m = 6.0$ and $R = 3.0$, respectively.

It follows from the data in Fig. 6 that the relative intensity at the side frequencies drops with increasing output power. At the same time, the absolute power of waves at the side frequencies, $P(\omega_0 \pm \Omega)$, increases owing to the increase in the power at the carrier frequency (total output power), $P(\omega_0)$. Moreover, at powers above 100 mW the $|V_{\pm1}(L)|^2$ values plateau. This suggests that further increasing the output power will cause no changes in modulation parameters. This behaviour is only due to the difference between the amplitude–phase coupling coefficients of the amplifier/modulator and power amplifier (R_m and R, respectively). This follows from Eqn (15) in Ref. [1] given that $|K| \to 0$ with increasing output power (with increasing u). The physical meaning of such behaviour is that mixed modulation of the input beam is converted into pure phase modulation in the power amplifier. Further amplification of the phase-modulated signal does not change its modulation parameters. This suggests that the dominant type of modulation in the diode power amplifier is phase modulation, whose depth is determined by the R of the gain medium of the amplifier and by the nature of the modulation (the relationship between the amplitude- and phase-modulated components) of the input signal. In our case, the nature of the modulation is determined by the parameter R_m. Only when R_m differs markedly from R can an optical signal be amplified in the diode power amplifier without changes in modulation depth.

Note that the Stokes and anti-Stokes components at the output of the amplifier/modulator have identical intensities, $V_{+1}(0)|^2 \equiv |V_{-1}(0)|^2 = |V(0)|^2$, as follows from Eqn (14) in Ref. [1]. Their phase relationships and, hence, the relationships between the amplitude- and phase-modulated components are determined by the amplitude–phase coupling coefficient R_m. If R differs from R_m, the output of the power amplifier will always contain a purely phase-modulated component, as reflected by the terms proportional to $R_m - R$ and $(R_m - R)^2$ in Eqn (15) in Ref. [1]. The term $(R_m - R)^2/(1 + R_m^2)$ determines the constant level the $|V_{\pm1}(L)|^2/|V(0)|^2$ ratio tends to as the amplifier output power increases.

The term proportional to $R_m - R$ causes the intensities of the Stokes and anti-Stokes components at the output to differ from each other. It also follows from calculation that, with increasing output power, the difference tends to zero, as would be expected in the case of a purely phase-modulated beam (Fig. 7).

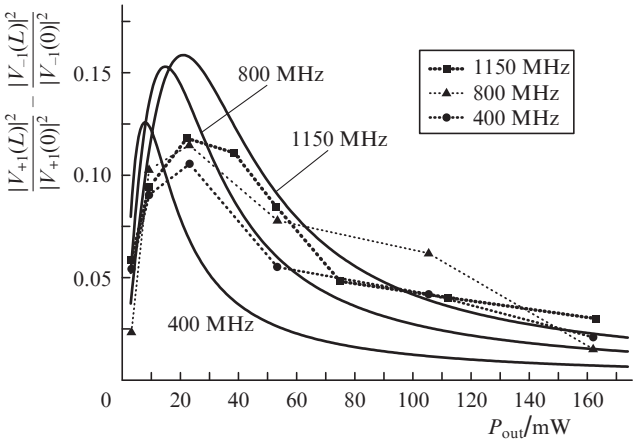

Figure 7. Difference between the relative changes in the absolute squares of the amplitudes of the anti-Stokes (Fig. 6b) and Stokes (Fig. 6a) components for amplification in the power amplifier at different input beam modulation frequencies and the same parameters as in Fig. 6. The points represent the experimental data and the solid lines show calculation results.

In this study, R_m and R differed owing to the difference between the operating points (direct component) of the pump current of the amplifier/modulator and power amplifier. The amplitude–phase coupling coefficient of a gain medium is known to depend on the pump intensity (carrier concentration in the active region) and wavelength (its position with respect to the central gain peak) (see e.g. Refs [7–9]). Therefore, varying the direct current through the amplifier/modulator, one can change R_m and, hence, the level the value of $|V_{\pm1}(L)|^2$ tends to. This is evidenced by the data in Figs 8 and 9. Previous experimental data [8, 9] suggest that increasing the pump current of the amplifier/modulator at a constant wavelength led to an increase in R_m from 4.3 to ~6.0.

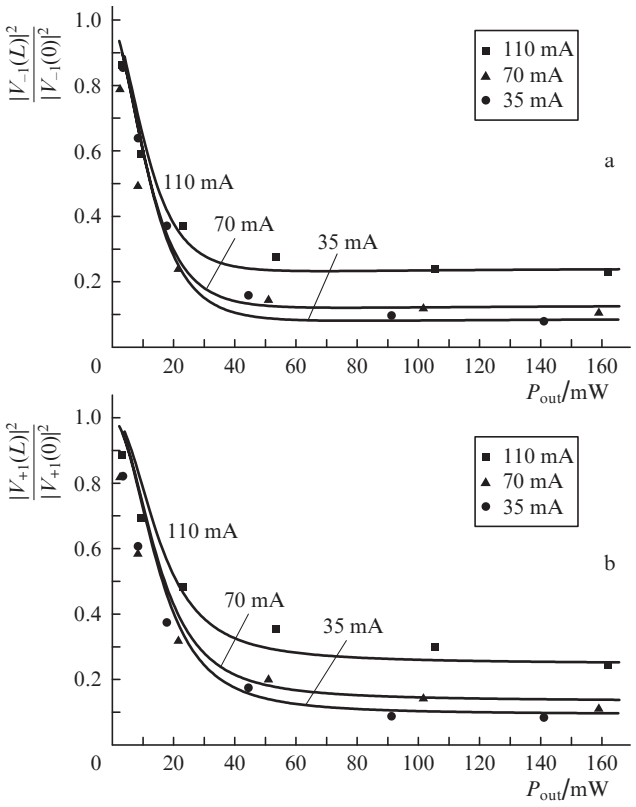

Figure 8. Relative change in the absolute squares of the amplitudes of the (a) Stokes and (b) anti-Stokes components for amplification in the power amplifier at different currents through the amplifier/modulator and a modulation frequency of 800 MHz. The points represent the experimental data and the solid lines show calculation results for R_m = 4.35, 4.75 and 6.0 at currents of 35, 70 and 110 mA, respectively. The R of the power amplifier is 3.0.

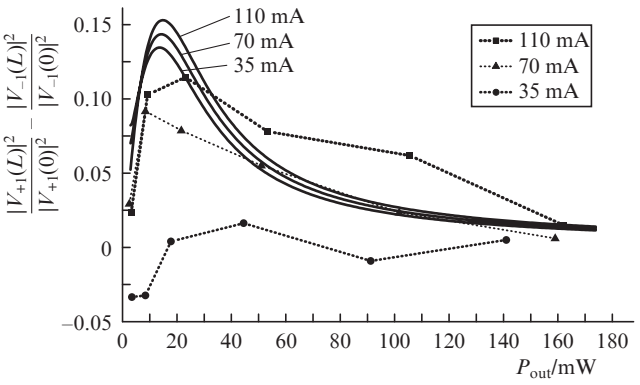

Figure 9. Difference between the relative changes in the absolute squares of the amplitudes of the anti-Stokes (Fig. 8b) and Stokes (Fig. 8a) components of the output beam at different currents through the amplifier/modulator and the same parameters as in Fig. 8. The points represent the experimental data and the solid lines show calculation results.

The slight deviation of the data points from the calculated curves in Figs 6 and 8 may be due not only to statistical errors but also to uncertainties in the parameters of the amplifier. For example, when determining the parameters we took $\Gamma_w = 1$, whereas the actual value may be ~0.8, which will of course entail some corrections to the parameters found above. Moreover, the curves were obtained in a model which assumed R to be constant along the length of the amplifier. Clearly, the actual value of R near the input facet may differ from that near the output facet of the amplifier. Therefore, the R_m and R used in our calculation should be taken to mean some values averaged over the length of the corresponding amplifiers.

Nevertheless, we think that the calculation results and experimental data in Figs 6 and 8 are in good agreement.

As to the difference in intensity between the Stokes and anti-Stokes components, the intensity of the anti-Stokes component was slightly higher in our case because $R_m > R$. At the same time, both calculation and experiment demonstrate that the difference is not very large: less than 10% (relative to the input intensity) in the maximum. Even though the experimental data in Figs 7 and 9 have a considerable scatter with respect to calculation results, we are confident that the scatter does not influence the conclusion that the anti-Stokes component prevails in our case and that the power of the components has a maximum (Figs 7, 9) at moderate output powers, as follows from calculation.

4. Discussion and conclusions

We have carried out what we believe to be the first experimental study of the propagation and amplification of a modulated beam in a diode power amplifier operating deep in saturation. We had to limit the output power of the amplifier to ~100 mW to avoid irreversible changes that otherwise might have been caused by optical damage to the output facet of the diode. Such a power limitation is not connected to the subject of this study, because it has a different physical nature and can be raised by independent methods. One example is work by Sverdlov et al. [10]: using optical hardening of the output facet and optimising the horizontal waveguide of a laser diode, they reached an output power of ~3 W in the steady-state single-transverse-mode regime. Given this, we believe that all the present results will remain in force or even will become better (e.g. the modulation band will become broader) as the output power of the amplifier will be increased further.

The results for the dynamic and static operation of the power amplifier fully confirm the adequacy of the theory presented in Ref. [2]: the calculation results obtained within this theory in Ref. [1] agree well with experimental data. Moreover, comparison of them allowed us to find parameters of the amplifier necessary for comprehensive modelling of its operation not only under the conditions considered above but also in a number of other instances. In particular, whereas under static conditions the measurand is the parameter $\sigma\tau$ (saturation intensity), under dynamic conditions the parameter $\Omega\tau$ appears together with this parameter. Determining the former parameter from the experimental data in Figs. 6 and 8, and using the $\sigma\tau$ found earlier, we can separately determine σ and τ, as was done in this study.

Experimental data demonstrate that the changes in the intensities at the side frequencies as a result of the nonlinear interaction of their fields with the field of the 'strong' carrier frequency depend on their phase relationships. A particular mechanism of interaction between fields through inversion and the dependence of the refractive index on carrier concentration lead to different results if there are different amplitude–phase relationships of fields at the amplifier input, as

shown earlier [11–14]. For example, if there is only one 'strong' field at the amplifier input and there is a 'weak' field in the Stokes region, whereas the anti-Stokes component is suppressed in some way (for example, because of the losses at this frequency or phase mismatch), the Stokes component will experience appreciable additional amplification by the strong field. In another case, when an input signal contains both the Stokes and anti-Stokes components, as a result of the same interaction a combination of the fields at the side frequencies that corresponds to amplitude modulation of the signal will be suppressed by the strong field at the centre frequency. By contrast, a field combination corresponding to a phase-modulated signal will not be influenced by the strong field upon amplification.

There is experimental evidence that efficient amplification of a modulated signal in a diode amplifier/modulator–diode power amplifier system is possible when the coefficients R_m and R differ markedly. The dominant type of amplified beam modulation is then phase modulation.

In our experiments, the input signal had identical intensities of waves at the side frequencies and their phase relationships were set by the amplitude–phase coupling coefficient R_m, which exceeded R. In that case, the output anti-Stokes component was slightly greater than the Stokes component. Calculations indicate that, in the opposite case ($R_m < R$), the output Stokes component may exceed the anti-Stokes component. Anyway, at a sufficiently high power the output intensities of the Stokes and anti-Stokes components become identical and their phase relationships correspond to a phase-modulated signal.

At $R_m = R$, the side components at the amplifier output will be suppressed. Their intensities will tend to zero with increasing amplifier output power. This means that, in our amplifier/modulator–output power amplifier system, an intense modulated optical beam can only be obtained at $R_m \neq R$. Moreover, in any case the output beam of the diode power amplifier will be predominantly phase-modulated, with a suppressed amplitude-modulated component.

In conclusion, note that the present results in combination with previous data [1] strongly suggest that diode lasers can be regarded as hardware components for creating highly efficient, small emitters for free-space communication systems with a multiwatt average output power of a phase-modulated beam and a near diffraction-limited beam divergence. The modulation bandwidth may be at a level of ~10 GHz for the amplification of an amplitude-modulated beam in the output power amplifier and above 100 GHz for the amplification of a phase-modulated beam.

Acknowledgements. This work was supported by the Russian Academy of Sciences (Theme No. 01201156501: Properties of Optoelectronic Materials and Structures and Possibilities of Using Them in Laser Engineering, Computer Technologies and Medical Applications) and in part by the Russian Foundation for Basic Research (Grant No. 12-02-31345 mol_A_2012) and the Educational–Scientific Complex, P.N. Lebedev Physics Institute, Russian Academy of Sciences.

References

1. D'yachkov N.V., Bogatov A.P., Gushchik T.I., Drakin A.E. *Kvantovaya Elektron.*, **44**, 997 (2014) [*Quantum Electron.*, **44**, 997 (2014)].
2. Bogatov A.P., D'yachkov N.V., Drakin A.E., Gushchik T.I. *Kvantovaya Elektron.*, **43**, 699 (2013) [*Quantum Electron.*, **43**, 699 (2013)].
3. Annenkov D.M., Bogatov A.P., Eliseev P.G., Okhotnikov O.G., Pak G.T., Rakhval'skii M.P., Fedorov Yu.F., Khairetdinov K.A. *Kvantovaya Elektron.*, **11**, 231 (1984) [*Sov. J. Quantum Electron.*, **14**, 163 (1984)].
4. Soskin, M.S., Taranenko V.B. *Kvantovaya Elektron.*, **4**, 536 (1977) [*Sov. J. Quantum Electron.*, **7**, 298 (1977)].
5. Plisyuk S.A., Batrak D.V., Drakin A.E., Bogatov A.P. *Kvantovaya Elektron.*, **36**, 1058 (2006) [*Quantum Electron.*, **36**, 1058 (2006)].
6. Lobintsov A.A., Uspenskii M.B., Shishkin V.A., Shramenko M.B., Yakubovich S.D. *Kvantovaya Elektron.*, **40**, 305 (2010) [*Quantum Electron.*, **40**, 305 (2010)].
7. Wenzel H., Erbert G. *IEEE J. Sel. Top. Quantum Electron.*, **5**, 637 (1999).
8. Bogatov A.P., Boltaseva A.E., Drakin A.E., Belkin M.A., Konyaev V.P. *Kvantovaya Elektron.*, **30**, 315 (2000) [*Quantum Electron.*, **30**, 315 (2000)].
9. Bogatov A.P., Boltaseva A.E., Drakin A.E., Belkin M.A., Konyaev V.P. *Fiz. Tekh. Poluprovodn.*, **34**, 1258 (2000).
10. Sverdlov B., Pfeiffer H.-U., Zibik E., et al. *Proc. SPIE Int. Soc. Opt. Eng.*, **8605**, 860508-1 (2013).
11. Bogatov A.P., Eliseev P.G., Sverdlov B.N. *IEEE J. Quantum Electron.*, **QE-11**, 510 (1975).
12. Bogatov A.P., Eliseev P.G., Okhotnikov O.G., Rakhval'skii M.P., Khairetdinov K.A. *Kvantovaya Elektron.*, **10**, 1851 (1983) [*Sov. J. Quantum Electron.*, **13**, 1221 (1983)].
13. Bogatov A.P., Eliseev P.G., Kobildzhanov O.A., Madgazin V.R. *IEEE J. Quantum Electron.*, **QE-23**, 1064 (1987).
14. Batrak D.V., Bogatov A.P., Kamenets F.F. *Kvantovaya Elektron.*, **33**, 941 (2003) [*Quantum Electron.*, **33**, 941 (2003)].